In vivo confocal and multiphoton microendoscopy

Pilhan Kim, Mehron Puoris'haag, Daniel Côté, Charles P. Lin, and Seok H. Yun*

Harvard Medical School and Massachusetts General Hospital, Wellman Center for Photomedicine, 50 Blossom St., BAR 818, Boston, Massachusetts 02114

Abstract. The ability to conduct high-resolution fluorescence imaging in internal organs of small animal models *in situ* and over time can make a significant impact in biomedical research. Toward this goal, we developed a real-time confocal and multiphoton endoscopic imaging system. Using 1-mm-diameter endoscopes based on gradient index lenses, we demonstrate video-rate multicolor multimodal imaging with cellular resolution in live mice. © *2008 Society of Photo-Optical Instrumentation Engineers.* [DOI: 10.1117/1.2839043]

Confocal and multiphoton microscopy, combined with fluorescent biomarkers, has opened up new avenues for biomedical investigations in small-animal models. These high-resolution technologies enable us to visualize a wide range of biological processes, such as molecular expression, cell trafficking, and cell-cell and cell-microenvironment interactions, in natural environment *in vivo*, providing information that cannot be obtained *in vitro* or *ex vivo*.[1–3] Until now, however, these techniques have almost exclusively been limited to surface imaging, either through the skin, surgically embedded optical windows, or extensive surgical exposure of tissue, because of limited light penetration in tissue and the relatively large size of standard high-numerical-aperture (NA) objective lens. The ability to conduct confocal and multiphoton microscopy safely and effectively in internal organs, *in vivo* and over time, would greatly increase the number of applications in basic and translational research.

Microendoscopy is a promising approach for internal organ imaging *in vivo*. It combines conventional intravital microscopy and miniature endoscopy, using a narrow-diameter optical probe that provides minimally invasive access to internal organs that are otherwise difficult to reach with conventional instruments. Developing high-resolution endoscopy has been driven largely by clinical applications.[4,5] Most endoscopic probes designed for human use, however, are suboptimal for small-animal imaging due to their relatively large size and insufficient resolution. Recently, several research groups have demonstrated promising endoscope technologies based on fiber optic bundles[6] and gradient-index (GRIN) lenses.[7–9] Confocal fiber bundles offer a relatively poor transverse res-
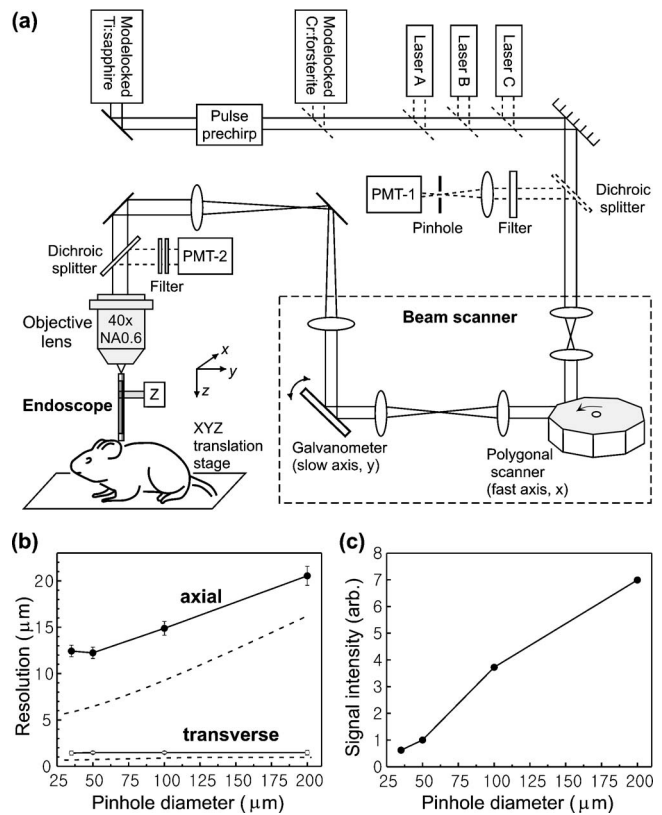

Fig. 1 (a) Schematic of the microendoscope imaging system and (b) spatial resolution and (c) signal strength in confocal microendoscopy measured with different pinhole sizes. Dotted lines in (b) represent theoretical diffraction-limited resolution of a 0.45-NA objective lens.

olution of 3 to 5 μm and may not be suitable for delivering short pulses for multiphoton imaging. In contrast, GRIN endoscopes have been demonstrated to have cellular resolution for one-photon (wide-field) and two-photon fluorescence imaging.[8,9] In this letter, we extend this approach by developing a real-time video-rate, multicolor multimodal microendoscope system. In particular, we describe a simple technique for overcoming chromatic aberration of GRIN lens to demonstrate the first confocal fluorescence microendoscopy, as well as second-harmonic generation (SHG) and two-photon fluorescence imaging, in live mice.

Our imaging system was built on a video-rate scanning laser confocal microscope platform previously developed[10] [Fig. 1(a)]. The system uses continuous-wave lasers at 491, 532, and 635 nm for single-photon fluorescence excitation and a mode-locked tunable Ti:sapphire (780 to 920 nm) and a Cr:forsterite laser (1240 nm) for multiphoton excitation. Flip mirrors and dichroic splitters were used to select and direct a laser beam to a raster beam scanner comprising a silver-coated polygon scanner (x axis) and a galvanometer (y axis). We designed the microscope to have a field of view (FOV) of 250×250 μm^2 when a $40\times$ objective lens (Olympus, LUCPlanF1; 0.6 NA; dry) is used. The proximal end of the endoscope is placed approximately at the focal plane of the objective lens. A confocal pinhole and a photomultiplier tube (PMT-1, Hamamatsu, R3896) were used for confocal fluores-

*Tel: 617–724–6152; E-mail: syun@hms.harvard.edu

cence and reflectance imaging, whereas another photomultiplier tube (PMT-2) was for two-photon fluorescence and SHG imaging. An 8-bit two-channel frame grabber digitizes the output of each PMT at 10 MS/s, acquiring 500×500 pixels/frame. The system acquires and displays images in real time at a frame rate of 30 Hz and can save them to hard disk simultaneously.

We designed and fabricated several endoscopes using 1-mm-diam commercial GRIN lenses (NSG and Grintech). Each endoscope has the same triplet structure as reported previously[11] comprising two high-NA (0.45 to 0.6) GRIN lenses (pitch: 0.16 to 0.25) and a half-pitch low-NA (0.1 to 0.2) relay lens in between. The endoscopes we used in the experiments described here are 15 mm long and have 0.45 imaging NA, an FOV diameter of 250 to 300 μm, and a working distance of ~300 μm with water immersion.

To measure the resolution, we imaged 200-nm-diam fluorescent polystyrene microbeads (Invitrogen) in a monolayer between a glass slide and a cover slip, as this sample was translated with a submicrometer step in the x, y, or z axis. In two-photon excitation imaging at 800 nm, the measured resolution was 1.1 ± 0.08 μm in x or y and 13.4 ± 0.3 μm in z, defined as full width at half maximum (FWHM). In confocal imaging, the pinhole diameter is an important parameter determining the resolution. Pinhole sizes greater than the Airy disk were previously used for deep tissue imaging.[10] Consistent with theory, we measured the transverse resolution to be relatively insensitive to the pinhole size and found a strong dependence for both axial resolution and signal strength [Figs. 1(b) and 1(c)]. All the confocal images presented in this letter were obtained using a pinhole with one Airy disk size (50 μm). This provided a resolution of 1.5 ± 0.08 μm in x or y and 12.4 ± 0.3 μm in z, comparable to that of two-photon imaging. These values are approximately twice larger than theoretical diffraction limits of 0.45-NA optics, which is attributed to spatial aberration of GRIN lenses. In addition to spatial aberration, we observed significant chromatic aberration in the endoscope. We measured that the focal depth was different between 491- and 635-nm excitation wavelengths by 35 to 90 μm, depending on the specific GRIN lenses used. Such a large variation of focus, corresponding to several cell layers, would be a significant problem frustrating multicolor-excitation cellular imaging. We solved this problem by a simple technique; whenever changing the excitation wavelength, we adjusted the vertical position of the objective lens by 35 to 90 μm accordingly so that the focal plane of the endoscope remains unchanged. Furthermore, we used an optimal pinhole position and bandpass emission filters to minimize image blur due to the wavelength differences between excitation and emission and within the emission band.

To test the imaging system, we imaged plant seeds stained with fluorescent dyes in a slide (Carolina Biological Supply). Figures 2(a) and 2(b) are fluorescence images of pollen grains acquired with confocal and two-photon endoscopy, respectively, showing micrometer-scale structures with reduced out-of-focus light by depth sectioning. These are compared with the image of the same sample taken directly using the 0.6-NA objective [Fig. 2(c)]. SHG imaging of a potato visualizes the boundaries of spherical starch granules [Fig. 2(d)]. Figures 2(e) and 2(f) are confocal images of a pine embryo acquired at excitation wavelengths of 491 and 635 nm, respectively,
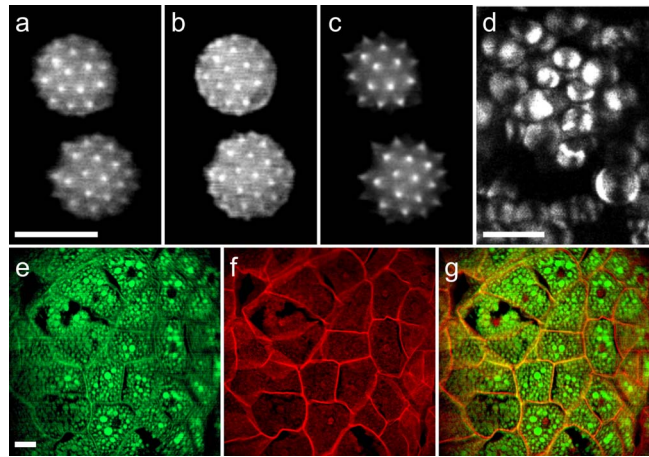

Fig. 2 Various images acquired with the imaging system. (a) to (c) Fluorescence images of a pollen grain sample. The images in (a) and (b) were obtained with a GRIN endoscope by two-photon excitation at 860 nm and by confocal excitation at 635 nm, respectively. The image in (c) was obtained by 860-nm two-photon excitation using a standard objective lens (40×, 0.6 NA), shown for comparison. (d) Endoscopic SHG image of starch in a sliced fresh potato. The polarization state of the excitation beam was linear along the horizontal axis. (e) and (f) Confocal endoscope images of a pine embryo [in (e), excitation; 491 nm, and emission; 520/35 nm; in (f) excitation; 635 nm, and emission; 692/40 nm]. (g) Merged image of (e) and (f). Image blurring near the FOV boundary is due to field curvature. Each image was averaged over 30 frames acquired in 1 s at the same sample position. Scale bars are 25 μm. (Color online only.)

using the chromatic-aberration compensation technique described earlier. A merged image [Fig. 2(g)] demonstrates coregistration of the red and green fluorescence images within a few micrometers over the nearly entire FOV.

To demonstrate *in vivo* tissue imaging, we conducted noninvasive confocal and multiphoton endoscopy of the skin in the ear of live mice. Using the GRIN endoscopes, we were able to visualize individual dendritic cells expressing green fluorescent proteins (GFP) in the epidermis and dermis [Fig. 3(a)], blood plasma labeled with rhodamine B-dextran conjugates [Fig. 3(b)], and collagen fibers via SHG in the dermis [Fig. 3(c)]. Video-rate monitoring not only greatly facilitates image navigation, but also allows monitoring fast dynamic processes such as cell trafficking in the blood stream. Figures 3(d)–3(f) show movie frames acquired by confocal microendoscopy from a GFP+ Tie-2 mouse after tail-vein injection of human ovarian cancer cells labeled with DiD *in vitro*. Individual cancer cells could be clearly distinguished in the circulation, and the cell density and the velocity can be measured. The maximum penetration depth was approximately 100 μm from the surface of the skin in all imaging modalities, limited by the SNR and the out-of-focus background.

In conclusion, we developed a multicolor multimodal microendoscope system and demonstrated real-time cellular imaging *in vivo* via a 1-mm-diam GRIN endoscope. We observed that, in most practical circumstances, confocal fluorescence imaging provided the brighter images and deeper penetration depth than two-photon fluorescence imaging, in part due to the limited imaging NA (0.45). The miniature microendoscopy described here may prove useful for biological investigations in small animals *in vivo*.
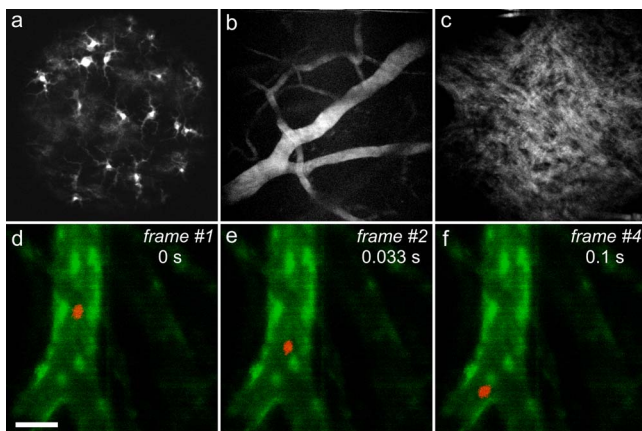
Fig. 3 Images of the intact ear skin in anesthetized mouse. (a) Confocal image showing Langerhans cells expressing GFP+ major histocmpatibility complex (MHC) class II molecules in a genetically engineered mouse [generously provided by Dr. Marianne Boes at Harvard Medical School (HMS)]. Excitation is 491 nm; emission is 520/35 nm. (b) Two-photon fluorescence image of blood vessels with free-flowing rhodamine-B-dextran conjugates after tail-vein injection (2,000,000 MW, 200 μg/200 μl). Excitation is 800 nm, 30 mW; emission is 590/80 nm. (c) Collagen fibrillar structure visualized by SHG. Excitation is 800 nm, 30 mW; emission is 417/60 nm. The images in (a) to (c) were averaged over 30 consecutive frames acquired in 1 s. (d) to (f) A sequence of frames showing ovarian cancer cells (OVCAR-1) in blood circulation, superimposed on a green fluorescence image of blood vessels in a GFP+ Tie2 mouse (generously provided by Dr. Scott Plotkin at HMS). The OVCAR-1 cells were labeled *in vitro* using DiD (Invitrogen) and injected at the tail vein [2 million cells in phosphate-buffered saline (PBS) 200 μl]. Scale bar is 50 μm. (Color online only.)

Acknowledgments

References

1. M. J. Miller, S. H. Wei, I. Parker, and M. D. Cahalan, "Two-photon imaging of lymphocyte motility and antigen response in intact lymph node," *Science* **296**, 1869–1873 (2002).
2. C. Halin, J. R. Mora, C. Sumen, and U. H. von Andrian, "In vivo imaging of lymphocyte trafficking," *Annu. Rev. Cell Dev. Biol.* **21**, 581–603 (2005).
3. D. A. Sipkins, X. Wei, J. W. Wu, J. M. Runnels, D. Cote, T. K. Means, A. D. Luster, D. T. Scadden, and C. P. Lin, "In vivo imaging of specialized bone marrow endothelial microdomains for tumour engraftment," *Nature (London)* **435**, 969–973 (2005).
4. R. Kiesslich, J. Burg, M. Vieth, J. Gnaendiger, M. Enders, P. Delaney, A. Polglase, W. McLaren, D. Janell, S. Thomas, B. Nafe, P. R. Galle, and M. F. Neurath, "Confocal laser endoscopy for diagnosing intraepithelial neoplasias and colorectal cancer in vivo," *Gastroenterology* **127**, 706–713 (2004).
5. C. MacAulay, P. Lane, and R. Richards-Kortum, "In vivo pathology: microendoscopy as a new endoscopic imaging modality," *Gastrointest Endosc Clin. N. Am.* **14**, 595–620 (2004).
6. E. Laemmel, M. Genet, G. Le Goualher, A. Perchant, J. F. Le Gargasson, and E. Vicaut, "Fibered confocal fluorescence microscopy (Cell-viZio) facilitates extended imaging in the field of microcirculation. A comparison with intravital microscopy," *J. Vasc. Res.* **41**, 400–411 (2004).
7. D. Bird and M. Gu, "Two-photon fluorescence endoscopy with a micro-optic scanning head," *Opt. Lett.* **28**, 1552–1554 (2003).
8. J. C. Jung, A. D. Mehta, E. Aksay, R. Stepnoski, and M. J. Schnitzer, "In vivo mammalian brain imaging using one- and two-photon fluorescence microendoscopy," *J. Neurophysiol.* **92**, 3121–3133 (2004).
9. M. J. Levene, D. A. Dombeck, K. A. Kasischke, R. P. Molloy, and W. W. Webb, "In vivo multiphoton microscopy of deep brain tissue," *J. Neurophysiol.* **91**, 1908–1912 (2004).
10. M. Rajadhyaksha, R. R. Anderson, and R. H. Webb, "Video-rate confocal scanning laser microscope for imaging human tissues in vivo," *Appl. Opt.* **38**, 2105–2115 (1999).
11. J. C. Jung and M. J. Schnitzer, "Multiphoton endoscopy," *Opt. Lett.* **28**, 902–904 (2003).